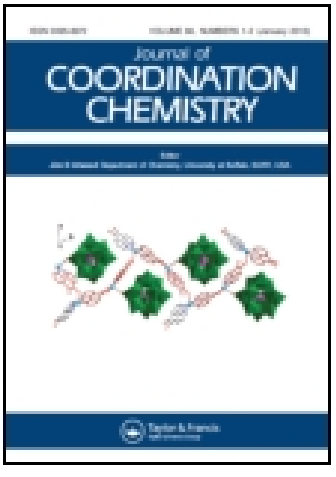

Journal of Coordination Chemistry
Publication details, including instructions for authors and subscription information:
http://www.tandfonline.com/loi/gcoo20

Synthesis, structures, and spectroscopic properties of Hg(II) complexes of bidentate NN and tridentate NNO Schiff-base ligands

Tushar S. Basu Baul[a], Sajal Kundu[a], Herbert Höpfl[b], Edward R.T. Tiekink[c] & Anthony Linden[d]

[a] Centre for Advanced Studies in Chemistry, North-Eastern Hill University, NEHU Permanent Campus, Shillong, India

[b] Centro de Investigaciones Químicas, Universidad Autónoma del Estado de Morelos, Cuernavaca, Mexico

[c] Department of Chemistry, University of Malaya, Kuala Lumpur, Malaysia

[d] Department of Chemistry, University of Zurich, Zurich, Switzerland

Accepted author version posted online: 05 Mar 2014.Published online: 08 Apr 2014.

To cite this article: Tushar S. Basu Baul, Sajal Kundu, Herbert Höpfl, Edward R.T. Tiekink & Anthony Linden (2014) Synthesis, structures, and spectroscopic properties of Hg(II) complexes of bidentate NN and tridentate NNO Schiff-base ligands, Journal of Coordination Chemistry, 67:6, 1061-1078, DOI: 10.1080/00958972.2014.901508

To link to this article: http://dx.doi.org/10.1080/00958972.2014.901508

Journal of Coordination Chemistry, 2014
Vol. 67, No. 6, 1061–1078, http://dx.doi.org/10.1080/00958972.2014.901508

Synthesis, structures, and spectroscopic properties of Hg(II) complexes of bidentate NN and tridentate NNO Schiff-base ligands

TUSHAR S. BASU BAUL*†, SAJAL KUNDU†, HERBERT HÖPFL‡, EDWARD R.T. TIEKINK*§ and ANTHONY LINDEN¶

†Centre for Advanced Studies in Chemistry, North-Eastern Hill University, NEHU Permanent Campus, Shillong, India
‡Centro de Investigaciones Químicas, Universidad Autónoma del Estado de Morelos, Cuernavaca, Mexico
§Department of Chemistry, University of Malaya, Kuala Lumpur, Malaysia
¶Department of Chemistry, University of Zurich, Zurich, Switzerland

(*Received 3 January 2014; accepted 18 February 2014*)

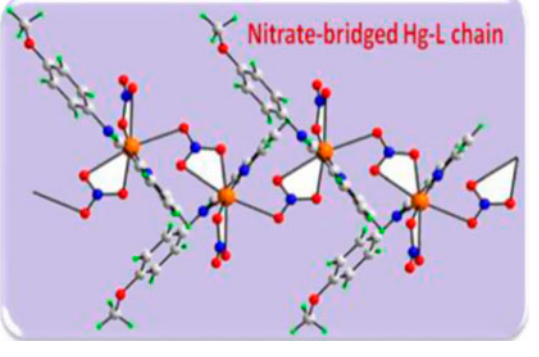

Depending on the formation of Hg–O bonds, monomeric (when present) or polymeric (absent) structures are formed in new Hg(Schiff-base)X_2(solvent) compounds.

Reactions of HgX_2 (X = Cl, N_3, NO_3) with (*E*)-2-methoxy-N-(pyridin-2-ylmethylene)aniline (L^1) and (*E*)-4-methoxy-N-(pyridin-2-ylmethylene)aniline (L^2) in ethanol gave two monomers, $[HgL^1(Cl)_2]$ (**1**) and $[HgL^2(NO_3)_2(DMSO)]$ (**5**), and three coordination polymers, $\{[HgL^1(N_3)_2]_2{\cdot}Hg(N_3)_2\}_n$ (**2**), $[HgL^2(Cl)_2]_n$ (**3**), and $[HgL^2(NO_3)_2]_n{\cdot}nCH_3CN$ (**4**). Compounds **1**–**5** were characterized by elemental analysis, IR, NMR spectroscopy, and single-crystal X-ray diffraction. The common feature of monomeric **1** and **5** is the presence of intra- and intermolecular Hg–O bonds. In the absence of these, polymeric structures arise as a result of azide, chloride, and nitrate bridging in **2**, **3**, and **4**, respectively. Fluorescent properties of **1**–**5** were also investigated.

*Corresponding authors. Email: basubaul@nehu.ac.in, basubaulchem@gmail.com (T.S. Basu Baul); Edward.Tiekink@gmail.com (E.R.T. Tiekink)

Keywords: Synthesis; Mercury(II) compounds; *N,N*-donor ligands; Photophysical properties; Crystal structures

1. Introduction

Schiff bases and their metal complexes have distinctive coordination and structural properties [1–5]. Schiff-base compounds of transition metals are important components for generation of supramolecular aggregates through formation of coordination bonds, hydrogen bonding, and other intermolecular interactions, thereby creating a variety of supramolecular architectures including high-dimensional frameworks [6–9]. X-ray crystallographic studies performed on a variety of mercury(II) compounds derived from Schiff-base ligands, viz. $HgLX_2$, $[HgLX_2]_2$, $[HgLX_2]_n$, and $\{[HgLX_2]_2\}_n$ with L = variously substituted (*E*)-N-(pyridin-2-ylmethylene)arylamine and X = halides or pseudohalides or nitrates, revealed that mercury(II) compounds are promising candidates for diverse supramolecular assemblies [10, 11]. Although the global topology (monomer, dimer, polymer, etc.) of the resulting compound is determined by the interplay between Hg^{2+}, X^-, and L, in the solid state, the crystal structure is frequently controlled by weaker intermolecular interactions such as π–π and CH–π contacts.

Herein, we report syntheses and solid-state structures of five new mercury(II) compounds derived from (*E*)-2-methoxy-N-(pyridin-2-ylmethylene)aniline (L^1) and (*E*)-4-methoxy-N-(pyridin-2-ylmethylene)aniline (L^2), which have been prepared from HgX_2 (X = Cl, N_3, and NO_3) (scheme 1) and then characterized by spectroscopic methods and single-crystal X-ray diffraction. The structural characterization shows formation of mononuclear or polymeric compounds. The coordination numbers range from 4 to 8, but are not systematically correlated to L^1/L^2 or X or solvent.

2. Experimental

2.1. *Materials, methods, and instruments*

Caution! Mercury compounds are highly toxic [12]. *Care must be taken when handling samples, and appropriate disposal procedures are necessary.* All chemicals were used as purchased: $HgCl_2$, NaN_3, pyridine-2-carboxaldehyde (Merck), $Hg(NO_3)_2$ (Sarabhai Chemicals), $Hg(OAc)_2$, *o*-anisidine, *p*-anisidine (Sd fine). (*E*)-2-methoxy-N-(pyridin-2-ylmethylene)aniline (L^1) and (*E*)-4-methoxy-N-(pyridin-2-ylmethylene)aniline (L^2) were generated *in situ* from pyridine-2-carboxaldehyde and the corresponding anisidine. Solvents were purified by standard procedures and freshly distilled prior to use. Melting points were recorded in capillary tubes on a Scanca apparatus and are uncorrected. Elemental analyses were performed using a Perkin Elmer 2400 series II instrument. IR spectra from 4000 to 400 cm^{-1} were obtained on a Perkin Elmer Spectrum BX series FT-IR spectrophotometer with samples as KBr disks. ^1H NMR spectra were recorded on a Bruker Avance II spectrometer and measured at 400.13 MHz, with chemical shifts referenced to Me_4Si set at δ 0.00 ppm; the numbering scheme is as shown in scheme 1. Steady-state absorption spectra were recorded at ambient temperature in acetonitrile (spectroscopy grade, Merck) solution on a Perkin-Elmer model Lambda25 absorption spectrophotometer. Fluorescence spectra were obtained on a Hitachi model FL4500 spectrofluorimeter (with excitation and emission

slits fixed at 10 and 20 nm, respectively). All spectra were corrected for instrument response function. Quartz cuvettes of 10 mm optical path length from Perkin Elmer, USA (part No. B0831009), and Hellma, Germany (type 111-QS), were used for measuring absorption and fluorescence spectra, respectively. Fluorescence quantum yields (ϕ_f) were calculated by comparing the total fluorescence intensity over the whole fluorescence spectroscopic range with that of a standard using the method described elsewhere [10]. The relative experimental error of the measured quantum yield was estimated within ±10%. Solution electrical conductivity measurements were made in acetonitrile with a Wayne Kerr automatic precision bridge 6440B.

2.2. *Synthesis of mercury compounds*

2.2.1. Synthesis of $[HgL^1(Cl)_2]$ (1). To a solution of pyridine-2-carboxaldehyde (0.13 g, 1.21 mM) in ethanol (5 mL) was added a solution of *o*-anisidine (0.15 g, 1.21 mM) in ethanol (5 mL). After stirring the reaction mixture at ambient temperature for 30 min, a solution of $HgCl_2$ (0.33 g, 1.21 mM) in methanol (20 mL) was added dropwise, which resulted in formation of a yellow precipitate. Stirring was continued for 3 h and then the mixture was filtered. The solid residue was washed with methanol (3 × 5 mL), dried *in vacuo* and then dissolved in 40 mL of hot acetonitrile. The solution was filtered while hot and upon cooling to room temperature, a yellow crystalline material was obtained. Yield 0.35 g (40%). M.p. 172–173 °C. Anal. Calcd for $C_{13}H_{12}Cl_2HgN_2O$ (MW 483.74): C, 32.28; H, 2.50; N, 5.79. Found: C, 32.60; H, 2.62; N, 5.80%. Λ_m (CH_3CN): 6 $\Omega^{-1}cm^2M^{-1}$. IR (cm^{-1}): 1623w, 1588s: $\nu(C{=}N_{imine} + C{=}N_{py})$, 1563w, 1492s, 1475w, 1462m, 1438w: $\nu(C{=}N_{py})$, 1368m, 1286w, 1269m, 1250 *versus*, 1178w, 1156w, 1156m, 1117 *versus*, 1047w, 1021m, 1011w, 972w, 958w, 942w, 903w, 774 *versus*, 759w, 744w, 638w, 617w, 537w, 508w. ^{1}HNMR (DMSO-d_6): 9.23 [s, 1H, H-7], 8.79 [d, 1H, H-3′], 8.19 [m, 2H, H-5′,6′], 7.84 [t, 1H, 4′], 7.60 [d, 1H, H-4], 7.43 [t, 1H, H-6], 7.10 [m, 2H, H-3,5], 4.0 [s, 3H, OCH_3] ppm.

2.2.2. Synthesis of $\{[HgL^1(N_3)_2]_2{\cdot}Hg(N_3)_2\}_n$ (2). *Note: While no incident occurred while using azide during preparation and isolation, care in handling azides must be exercised owing to their potentially explosive nature.* To a solution of pyridine-2-carboxaldehyde (0.25 g, 2.33 mM) in ethanol (5 mL) was added a solution of *o*-anisidine (0.28 g, 2.32 mM) in ethanol (5 mL). The mixture was stirred at ambient temperature for 30 min and then added dropwise to a methanolic solution containing HgN_3, which was prepared *in situ* from $Hg(OAc)_2$ (1.11 g, 3.48 mM) in methanol (50 mL) and NaN_3 (0.68 g, 10.46 mM) in 40 mL of the same solvent. Immediate formation of a yellow precipitate occurred. Stirring was continued for 4 h and then the mixture was filtered. The residue was washed thoroughly with water, then with methanol (3 × 5 mL) and dried *in vacuo*. The dried solid was dissolved in 60 mL of hot acetonitrile and filtered while hot. Upon cooling to room temperature, a yellow crystalline material was obtained. Yield 0.39 g (56%). M.p. 145–146 °C. Anal. Calcd for $C_{26}H_{24}Hg_3N_{22}O_2$ (MW 1278.39): C, 24.43; H, 1.89; N, 24.10. Found: C, 24.66; H, 1.80; N, 23.92%. Λ_m (CH_3CN): 5 $\Omega^{-1}cm^2M^{-1}$. IR (cm^{-1}): 2037 *versus*: $\nu_{as}(N_3)$, 1623s: $\nu(C{=}N_{imine})$, 1589m, 1496m, 1471w, 1458w: $\nu(C{=}N_{py})$, 1434w, 1371m, 1287w, 1272w, 1253s, 1193w, 1149w, 1119 *versus*, 1053w, 1021m, 1011w, 972w, 952w, 932w, 901w, 773m, 754w, 637w, 535w, 505w. ^{1}HNMR (DMSO-d_6): 8.94 [s, 1H, H-7],

8.73 [d, 1H, H-3′], 7.98 [m, 2H, H-5′,6′], 7.59 [t, 1H, 4′], 7.33 [d, 1H, H-4], 7.28 [t, 1H, H-6], 6.98 [m, 2H, H-3,5], 3.92 [s, 3H, OCH_3] ppm.

2.2.3. Synthesis of $[HgL^2(Cl)_2]_n$ (3). A similar synthetic procedure as for **1** was used except that *o*-anisidine was replaced by *p*-anisidine, giving yellow crystals after recrystallization from acetonitrile. Yield 0.30 g (49%). M.p. 192–193 °C. Anal. Calcd for $C_{13}H_{12}Cl_2HgN_2O$ (MW 483.74): C, 32.28; H, 2.50; N, 5.79. Found: C, 32.35; H, 2.42; N, 6.07%. Λ_m (CH_3CN): 7 $\Omega^{-1}cm^2\,M^{-1}$. IR (cm^{-1}): 1621w: ν(C=N_{imine}), 1596s, 1505 *versus*, 1473w, 1434w: ν(C=N_{py}), 1307m, 1251 *versus*, 1171m, 1029 *versus*, 835s, 776s, 537m. ^{1}HNMR (DMSO-d_6): 9.05 [s, 1H, H-7], 8.93 [d, 1H, H-3′], 8.13 [d, 2H, H-5′,6′], 7.75 [t, 1H, 4′], 7.65 [d, 2H, H-2,6], 7.00 [d, 2H, H-3,5], 3.85 [s, 3H, OCH_3] ppm.

2.2.4. Synthesis of $[HgL^2(NO_3)_2]_n \cdot nCH_3CN$ (4). $Hg(NO_3)_2$ (0.60 g, 1.46 mM) was dissolved under heating in five drops of concentrated nitric acid and the resulting solution was diluted with water (10 mL). This mixture was added dropwise to a solution containing pyridine-2-carboxaldehyde (0.155 g, 1.45 mM) and *p*-anisidine (0.179 g, 1.45 mM) in ethanol (10 mL), which resulted in the immediate formation of a yellow precipitate. Stirring was continued for 3 h and then the mixture was filtered. The residue was washed thoroughly with water until the filtrate was pH neutral, then with methanol (3 × 5 mL) and dried *in vacuo*. The dried solid was dissolved in 60 mL of hot acetonitrile and filtered while hot. The filtrate upon cooling to room temperature afforded **4** in the form of a pale yellow crystalline material. Yield 0.50 g (56%). M.p. 150–151 °C. Anal. Calcd for $C_{15}H_{15}HgN_5O_7$ (MW 577.90): C, 31.18; H, 2.62; N, 12.12. Found: C, 31.20; H, 2.42; N, 11.90%. Λ_m (CH_3CN): 9 $\Omega^{-1}cm^2\,M^{-1}$. IR (cm^{-1}) KBr: 1623w: ν(C=N_{imine}), 1594s, 1559m, 1507s, 1496m, 1447w: ν(C=N_{py}), 1384 *versus*, 1306w: $\nu(NO_3)$, 1257 *versus*, 1172m, 1117w, 1018m, 984m, 831s, 776m, 743w, 612w, 539w, 518w; Nujol: 1593 ν(C=N_{imine} + C=N_{py}), 1527 $\nu_1(NO_3)$, 1314 $\nu_5(NO_3)$. ^{1}HNMR (DMSO-d_6): 9.35 [d, 1H, H-3′], 8.93 [s, 1H, H-7], 8.40 [t, 1H, H-5′], 8.23 [d, 1H, 6′], 8.03 [t, 1H, H-4′], 7.52 [d, 1H, H-2,6], 6.97 [d, 2H, H-3,5], 3.84 [s, 3H, OCH_3] ppm.

2.2.5. Synthesis of $[HgL^2(NO_3)_2(DMSO)]$ (5). Crystallization of **4** in DMSO and chloroform (1:4, v/v) afforded pale yellow crystals of **5** in 56% yield. M.p. 165–166 °C. Anal. Calcd for $C_{15}H_{18}HgN_4O_8S$: C, 29.28; H, 2.95; N, 9.11. Found: C, 29.50; H, 3.08; N, 9.10%. Λ_m (CH_3CN): 9 $\Omega^{-1}cm^2\,M^{-1}$. IR (cm^{-1}) KBr: 1621w: ν(C=N_{imine}), 1595m: ν(C=N_{py}), 1579w, 1559w, 1507m, 1384 *versus*: $\nu(NO_3)$, 1320w, 1308w, 1254 *versus*, 1170m, 1158w, 1103w, 1021s: ν(S=O), 948m, 831s, 781m, 639w, 537w. ^{1}H-NMR (DMSO-d_6): 9.34 [d, 1H, H-3′], 8.95 [s, 1H, H-7], 8.39 [t, 1H, H-5′], 8.29 [d, 1H, 6′], 8.00 [t, 1H, H-4′], 7.55 [d, 1H, H-2,6], 7.02 [d, 2H, H-3,5], 3.84 [s, 3H, OCH_3], 3.46 [s, 6H, $(CH_3)_2SO$)] ppm.

2.3. *X-ray data collection and structure determination*

Crystals suitable for single-crystal X-ray diffraction analysis were obtained from a solvent mixture of acetone/acetonitrile (**1**), acetonitrile (**2–4**), and a solvent mixture of dimethylsulfoxide and chloroform (**5**) by slow evaporation of the solvent at room temperature. The

crystal for **1** was investigated at room temperature on a Bruker APEX diffractometer equipped with a CCD area detector (Mo Kα radiation with λ = 0.71073 Å, graphite monochromator). Data for **2** and **3** were recorded at low temperature on an Agilent Technologies SuperNova area-detector diffractometer [13] using Mo-Kα radiation (λ = 0.71073 Å) from a micro-focus X-ray source and an Oxford Instruments Cryojet XL cooler. Measurements for **4** and **5** were made at low temperature on a Nonius KappaCCD diffractometer [14] with graphite-monochromated Mo-Kα radiation (λ = 0.71073 Å) and an Oxford Cryosystems Cryostream 700 cooler. Data reduction was performed with SAINT [15] for **1**, with CrysAlisPro [13] for **2** and **3**, and HKL Denzo and Scalepack [16] for **4** and **5**. Intensities were corrected for Lorentz and polarization effects. An empirical absorption correction based on the multi-scan method [17] was applied for **1**, **4**, and **5**; the data for **3** were treated with an empirical absorption correction using spherical harmonics [13], and for **2** an analytical absorption correction [18] was employed. Relevant data collection and refinement parameters are given in table 1 and perspective views of the structures are shown in figures 2, 4, 5(a), 6(a), and 7(a). The structures of **1**, **4**, and **5** were solved by heavy-atom Patterson methods [19] which revealed the position of the mercury atom. The structures of **2** and **3** were solved by direct methods using SHELXS97 [20], giving the positions of all non-hydrogen atoms. In **1**, the asymmetric unit consists of two independent mononuclear molecules. The asymmetric unit in **4** contains one chemical repeat unit of the Hg-complex polymer plus one molecule of MeCN. Refinement of each structure was carried out on F^2 using full-matrix least-squares procedures, which minimized $\Sigma w(F_o^2 - F_c^2)^2$. The non-hydrogen atoms in each structure were refined anisotropically. All hydrogen atoms were placed in geometrically calculated positions and refined using a riding model, where each hydrogen atom was assigned a fixed isotropic displacement parameter with a value of $1.2U_{eq}$ of its parent atom ($1.5U_{eq}$ for any methyl group). A correction for secondary extinction was applied for **4** and **5**. Three reflections for **1** and one reflection for each of **4** and **5** were omitted from the final refinement, because the intensities were considered to be extreme outliers. The structure of **5** was refined as an inversion twin in which the major twin fraction was 0.859(1). With the exception of the positive residual electron density peaks, table 1, in **3** (1.18 Å from Cl2) and **4** (1.24 Å from C2), the maximum and minimum residual electron density peaks in the final difference maps were located in the vicinity of a mercury(II) atom. Refinement and data output of **1** were carried out with the SHELXTL-NT program package [20], while the SHELXL97 program [21] was used for the calculations of **2**–**5**. All crystallographic figures were drawn using SHELXTL-NT [20] or DIAMOND [22].

3. Results and discussion

3.1. *Syntheses*

Reactions for formation of the mercury Schiff base compounds **1**, **3**, and **4** were carried out in methanol or ethanol using 1 : 1 stoichiometric ratios. In either solvent, one equivalent of HgX_2 (X = Cl, NO_3) reacts rapidly with one equivalent of L (generated *in situ* from pyridine-2-carboxaldehyde and *o/p*-anisidine) to give a yellow precipitate, from which mercury(II) compounds, $[HgL^1(Cl)_2]$ (**1**), $[HgL^2(Cl)_2]_n$ (**3**), and $[HgL^2(NO_3)_2]_n{\cdot}nCH_3CN$ (**4**), were isolated. The combination of **4** with DMSO resulted in the formation of $[HgL^2(NO_3)_2(DMSO)]$ (**5**). Earlier, it was demonstrated that reaction of one equivalent of $Hg(N_3)_2$ with one

Table 1. Crystal data, data collection, and refinement parameters for **1–5**.

	1	**2**	**3**	**4**	**5**
Empirical formula	$C_{13}H_{12}Cl_2HgN_2O$	$C_{26}H_{24}Hg_3N_{22}O_2$	$C_{13}H_{12}Cl_2HgN_2O$	$C_{13}H_{12}HgN_4O_7{\cdot}CH_3CN$	$C_{15}H_{18}HgN_4O_8S$
Formula weight	483.74	1278.12	483.77	577.81	614.89
Crystal size (mm)	0.12 × 0.14 × 0.49	0.15 × 0.23 × 0.28	0.14 × 0.18 × 0.30	0.05 × 0.18 × 0.30	0.05 × 0.08 × 0.35
Crystal morphology	Block	Prism	Prism	Plate	Needle
Temperature (K)	293(2)	160(1)	160(1)	160(1)	160(1)
Crystal system	Orthorhombic	Triclinic	Monoclinic	Orthorhombic	Triclinic
Space group	*Pbca*	$P\bar{1}$	$P2_1/c$	*Pbca*	$P\bar{1}$
a (Å)	8.8128(13)	8.50515(18)	9.29317(17)	16.3111(2)	8.0022(1)
b (Å)	21.657(3)	9.7632(3)	7.10215(11)	9.4077(1)	10.2965(2)
c (Å)	30.600(4)	11.5385(3)	20.6719(4)	24.1767(4)	13.0245(3)
α (°)	90	67.645(3)	90	90	112.4632(8)
β (°)	90	79.274(2)	95.0498(17)	90	94.3431(11)
γ (°)	90	82.950(2)	90	90	95.3738(11)
V (Å^3)	5840.3(15)	869.22(4)	1359.08(4)	3709.91(9)	980.09(3)
Z	16	1	4	8	2
D_x (g cm^{-3})	2.201	2.441	2.364	2.069	2.083
μ (mm^{-1})	10.899	13.307	11.734	8.365	8.027
θ range (°)	2.3–25.0	2.3–32.5	2.2–29.5	2.5–27.5	2.2–30.1
Reflections measured	40,015	21,265	15,755	53,425	22,892
Indep. reflections; R_{int}	5142; 0.086	5774; 0.038	3405; 0.037	4247; 0.115	5654; 0.074
Reflections with $I > 2\sigma(I)$	3543	5262	3177	2979	5211
Number of parameters	345	243	174	255	266
$R(F)$ [$I > 2\sigma(I)$refIns]	0.037	0.027	0.028	0.040	0.028
$wR(F^2)$ (all data)	0.087	0.069	0.067	0.107	0.064
GOF(F^2)	1.00	1.10	1.17	1.02	1.07
$\Delta\rho_{max,\ min}$ (e, Å^{-3})	0.84, −0.59	2.89, −1.54	2.14, −1.15	2.16, −1.82	1.28, −1.45

equivalent of L, where L = (*E*)-4-methyl-N-(pyridin-2-ylmethylene)aniline, gives a yellow product $\{[HgL(N_3)_2]_2\}_n$ [10]. Now, a compound of composition $\{[HgL^1(N_3)_2]_2{\cdot}Hg(N_3)_2\}_n$ (**2**) was isolated from a reaction of L^1 with an excess of $Hg(N_3)_2$. Compound **2** is trinuclear and can be considered as an adduct formed between a dimeric $[HgL^1(N_3)_2]_2$ complex and $Hg(N_3)_2$. Compounds **1–5** are air-stable and behave as non-electrolytes in acetonitrile solution (see Section 2.2). The structures and geometries of **1–5** are detailed in scheme 1. The results of the crystal structure determinations of **1–5** (see Section 3.3) are consistent with the chemical and spectroscopic analyses.

3.2. *IR, NMR, UV–vis and fluorescence spectroscopy*

The infrared spectroscopic assignments of selected bands for **1–5** are given in Section 2.2. All compounds display a moderately intense band at 1590–1620 cm^{-1}, which is characteristic for $\nu(C{=}N_{imine})$ of metal-coordinated Schiff base ligands [10, 11, 23]. In addition, well-resolved sharp bands of variable intensity at 1600–1580, 1490–1475, and 1450–1435 cm^{-1} were assigned to metal-coordinated pyridine rings [10, 11, 23–25]. The azide and nitrate compounds **2**, **4**, and **5** have additional features. Compound **2** has a very strong band at 2037 cm^{-1} corresponding to $\nu_{as}(N_3)$ [26, 27]. A similar observation was recently noted for $\{[HgL(N_3)_2]_2\}_n$, where L = (*E*)-4-methyl-*N*-(pyridin-2-ylmethylene)aniline [10]. Complex **4** displays a strong band at 1384 cm^{-1}, indicative of the simultaneous presence of non-coordinated and coordinated nitrates [24, 28]. The KBr spectrum of **4** also displayed bands at 1507 and 1306 cm^{-1}, indicative of bidentate chelating nitrates. The bidentate chelating nitrates [24] were further confirmed from the spectrum of **4** run in Nujol mull, with bands at 1527 cm^{-1} for $\nu_1(NO_3)$ and at 1314 cm^{-1} for $\nu_5(NO_3)$, corresponding to a difference of $\Delta(NO_3)$ = 213 cm^{-1} [29]. A similar observation was made recently for an analogous mercury compound, $[HgL(NO_3)_2]_n$, which has also been characterized crystallographically [10]. In addition to bands for nitrate groups, **5** displayed a strong band at 1021 cm^{-1}, attributed to $\nu(S{=}O)$ of DMSO coordinated to mercury(II). This value is 35 cm^{-1} lower than that reported for free DMSO (1055 cm^{-1}) and is thus indicative of a terminal (end-on) O-monocoordination. For S-bonded DMSO, an increase in frequency would be expected [30, 31]. Thus, IR spectroscopic data provided substantial evidence in support of the structures which were subsequently confirmed by single crystal X-ray crystallography (see Section 3.3).

^{1}H NMR spectra for **1–5** in DMSO-d_6 solution displayed the expected signals, which correlate well with the hydrogen atoms present in the molecules. Coupling constants could not be established with certainty, owing to the broad unresolved nature of the signals. The NMR assignments for the compounds presented in the Experimental section are based on splitting patterns of the signals and by comparing the data with those in previous reports [32, 33].

Table 2. Photophysical data for **1–5** in acetonitrile.

Compounds	Electronic spectroscopic data λ_{max} (nm); (ε[M^{-1} cm^{-1}])	Photoluminescence data	
		λ_{em} (nm)[a]	ϕ_F
1	359 (12,096)	413, 427, 502	0.11
2	346 (22,109)	413, 429	0.08
3	378 (17,937)	412, 430	0.10
4	382 (11,390)	411, 431	0.12
5	382 (9305)	412, 429	0.09

[a]The long wavelength emission appears as a shoulder in all cases.

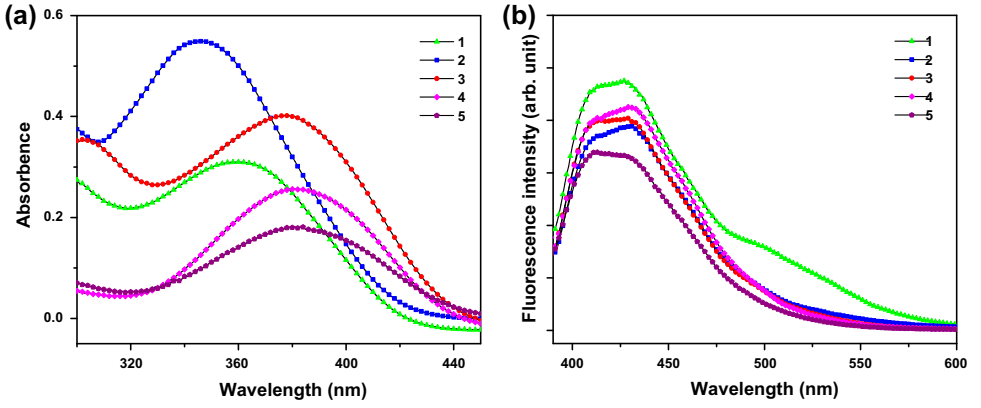

Figure 1. (a) UV–vis (concentration 10^{-3} M) and (b) fluorescence spectra (concentration ~10^{-5} M) obtained by excitation at the respective absorption maxima (table 2) of **1–5** in acetonitrile.

Table 2 summarizes the UV–vis and fluorescent properties of **1–5**. The electronic spectra exhibit a strong absorption at 350–380 nm [figure 1(a)], which is possibly a result of overlap of intramolecular charge transfer transitions (ε ~10^4) with a weak MLCT transition from Hg(II) → π^* (ligand) [10, 11]. In acetonitrile, compounds display broad emission bands at λ_{max} = 410 nm along with a shoulder at ~430 nm, except for an additional band at 502 nm for **1**, when they are excited at their respective absorption maxima [figure 1(b)], indicating the charge transfer nature of the transitions [10, 11]. Compounds **1–5** show very low fluorescent quantum yields (ϕ_F), which can be attributed to the heavy-atom effect [34, 35] and the ϕ_F values were of the same order of magnitude as observed recently for related systems [10, 11]. No appreciable change in ϕ_F was noticed as a result of variation of the substituents in the ligands from 2-OCH_3 (**1** and **2**) to 4-OCH_3 (**3–5**) or variation of the anion (chloride, azide, and nitrate).

3.3. *Single-crystal X-ray diffraction studies*

The crystal structures of **1–5** were established by X-ray crystallography which revealed the presence of monomeric **1**, **3**, and **5** and polymeric **2** and **4** species in the solid state. Two independent monomers comprise the asymmetric unit of **1**; these monomers are similar to a first approximation [figure 2(a) and (b)]; geometric parameters for the first independent molecule of **1** are collated in table 3. The mercury(II) atom is five coordinate, being bound by a tridentate L^1 ligand which chelates the metal atom via the nitrogen atoms while simultaneously forming a Hg–O bond; the coordination environment is completed by two chloride ligands. As observed in related structures [10, 11], the Hg–N(pyridyl) bond length is shorter than the Hg–N(imine) bond. The chelate ring is planar in both molecules, exhibiting r.m.s. deviations of 0.016 and 0.029 Å, respectively. However, this planarity does not extend over the entire L^1 as seen in the dihedral angles formed between the outer six-membered rings of 32.2(5)° and 29.5 (4)°, respectively, there being a twist about the imine-N–C(methoxyphenyl) bond; the C6–N2–C7–C8 and C26–N22–C27–C28 torsion angles are 29.3(12)° and 23.0(11)°, respectively. This difference between the independent molecules is highlighted in the overlay diagram [36] [figure 3(a)]. Similar ligand conformations are found in **2–5**. Based on τ = 0.23, the trigonality

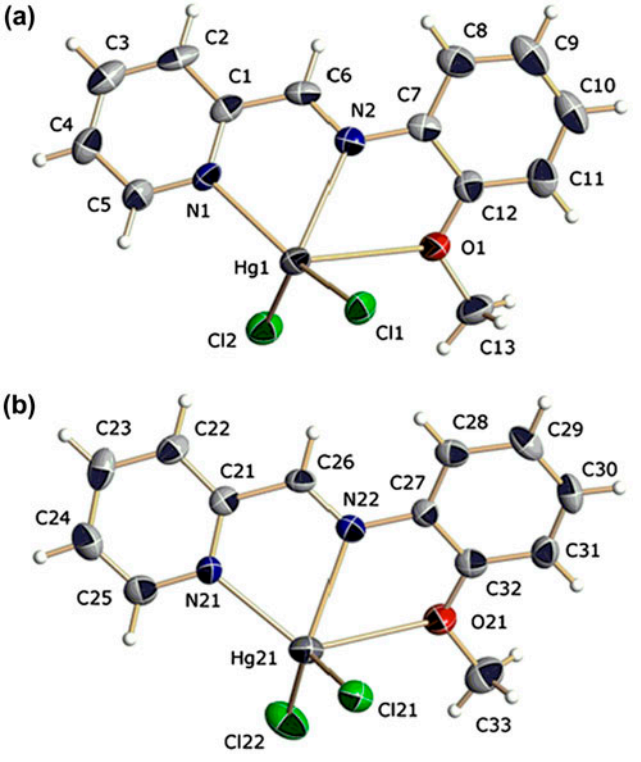

Figure 2. Perspective views of the two crystallographically independent monomers (a) and (b) found in the crystal structure of $[HgL^{1}(Cl)_2]$ (**1**). Displacement ellipsoids are drawn at the 30% probability level and hydrogen atoms are shown as small spheres of arbitrary radii.

Table 3. Selected bond lengths (Å) and angles (°) for **1** and **3**.[a]

	1	**3**		**1**	**3**
Hg(1)–Cl(1)	2.374(2)	2.4061(12)	Cl(2)–Hg(1)–N(1)	91.02(18)	98.89(10)
Hg(1)–Cl(2)	2.446(2)	2.5597(11)	Cl(2)–Hg(1)–N(2)	114.90(15)	100.07(9)
Hg(1)–N(1)	2.324(6)	2.260(4)	N(1)–Hg(1)–N(2)	69.1(2)	69.99(13)
Hg(1)–N(2)	2.473(6)	2.557(4)	Cl(1)–Hg(1)–Cl(2′)	–	95.09(4)
Hg(1)–Cl(2′)	–	2.7874(11)	Cl(2)–Hg(1)–Cl(2′)	–	100.77(2)
C(1)–C(6)	1.449(12)	1.454(7)	N(1)–Hg(1)–Cl(2′)	–	88.32(10)
N(2)–C(6)	1.259(10)	1.287(6)	N(2)–Hg(1)–Cl(2′)	–	151.92(9)
N(2)–C(7)	1.406(10)	1.422(6)	Hg(1)–Cl(2)–Hg(1″)	–	128.57(5)
			Hg(1)–N(1)–C(1)	118.4(6)	119.1(3)
Cl(1)–Hg(1)–Cl(2)	125.35(8)	106.62(4)	Hg(1)–N(1)–C(5)	122.3(6)	121.8(3)
Cl(1)–Hg(1)–N(1)	139.01(17)	153.09(10)	Hg(1)–N(2)–C(6)	113.6(6)	110.7(3)
Cl(1)–Hg(1)–N(2)	105.06(17)	96.77(9)	Hg(1)–N(2)–C(7)	124.2(5)	128.0(3)

[a]Symmetry operations for primed and doubly primed atoms = $1-x$, $\frac{1}{2}+y$, $1\frac{1}{2}-z$, and $1-x$, $-\frac{1}{2}+y$, $1\frac{1}{2}-z$, respectively.

index [37], compared with 0.0 and 1.0 for ideal square pyramidal and trigonal bipyramidal geometries, respectively, the coordination geometry about atom Hg1 is based on a square pyramid. The comparable value for the second molecule is 0.02, suggesting a more regular coordination geometry. The greater distortion for atom Hg1 is traced to a secondary Hg1···Cl21[i]

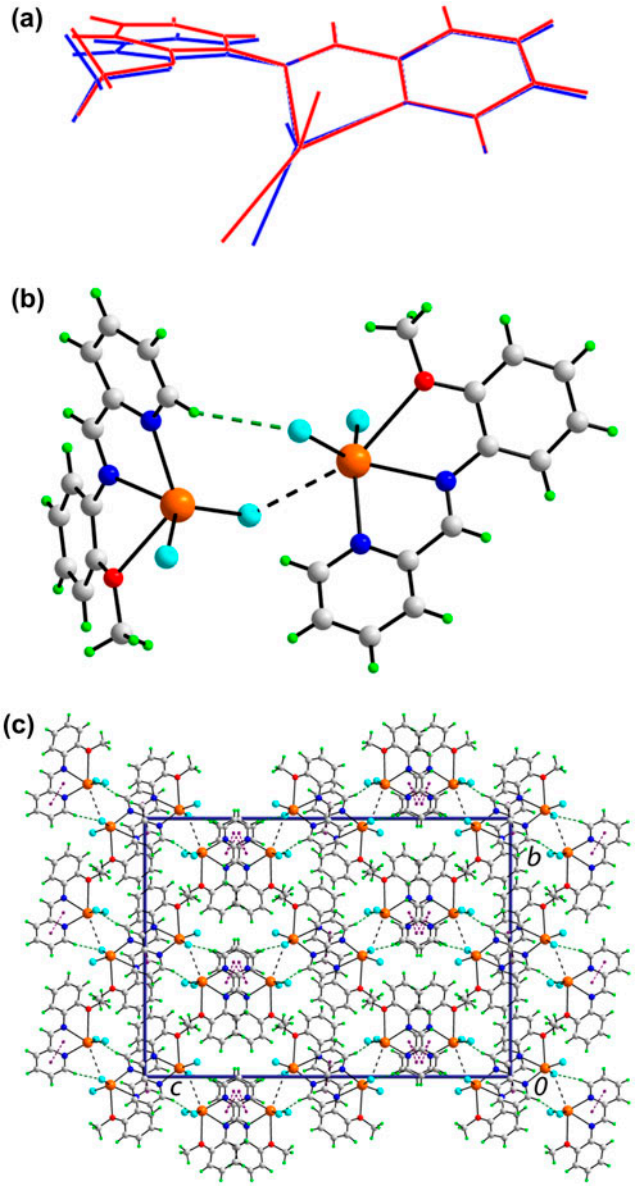

Figure 3. (a) Overlay diagram of the two independent molecules in $[HgL^1(Cl)_2]$ (**1**) (red image contains Hg1) superimposed so that the HgN_2C_2 rings are overlapped. (b) Illustration of the secondary Hg···Cl bonding [black dashed line, 3.309(2) Å] connecting the two independent molecules as well as the C–H···Cl hydrogen bond [green dashed line; H···Cl = 2.79 Å]. (c) View in projection down the *a*-axis of the unit cell contents. The C–H···Cl hydrogen bonds [C5–H5···Cl21^{i}: H5···Cl21^{i} = 2.82 Å, C5···Cl21^{i} = 3.502(10) Å, angle at H5 = 131° for i: −1 + *x*, −1 + *y*, *z*; C25–H25···Cl2^{ii}: H25···Cl2^{ii} = 2.79 Å, C25···Cl2^{ii} = 3.467(9) Å, angle at H25 = 130° for ii: 1 + *x*, 1 + *y*, *z*] and *π*–*π* interactions [Cg(N21,C21–C25)···Cg(N21,C21–C25)^{iii} = 3.484(5) Å for iii: 1 − *x*, 2 − *y*, −*z*; Cg(Hg1,N1,N2,C1, C6)···Cg(N1,C1–C5)^{iv} = 3.744(5) Å, angle of inclination = 7.9(4)° for iv: ½ + *x*, *y*, ½−*z*] are shown as green and purple dashed lines, respectively (see http://dx.doi.org/10.1080/00958972.2014.901508 for color version).

interaction of 3.309(2) Å (symmetry operation i: $-1+x$, $-1+y$, z) between independent molecules as shown in figure 3(b). Often molecules related to **1** dimerize about a center of inversion via Hg···Cl bridges to form binuclear arrangements [10, 11]. In the case of **1**, the presence of Hg–O bonds reduced the Lewis acidity of mercury(II) and only a single and weak Hg···Cl contact between the molecules is formed. Also highlighted in figure 3(b) is the presence of a pyridyl-C–H···Cl hydrogen bond [H···Cl = 2.79 Å]. In the crystal structure of **1**, there are two such pyridyl-C–H···Cl interactions and these, coupled with the Hg···Cl interaction, link the molecules into an array in the *bc*-plane. A 3-D architecture arises from π–π interactions along the *a*-direction between centrosymmetrically related N21-pyridyl rings, and between N21-pyridyl and $Hg1N_2C_2$ chelate rings [figure 3(c)]. The latter π–π interactions where a chelate ring defines a π-system are known [38–40] and indeed, have been seen in related structures [10, 11].

The structure of $\{[HgL^1(N_3)_2]_2{\cdot}Hg(N_3)_2\}_n$ (**2**) is best described as comprising a $Hg(N_3)_2$ unit and a centrosymmetric dimer of $[HgL^1(N_3)_2]_2$ with links provided by azido-N atoms (figure 4). The Hg2 atom in $Hg(N_3)_2$ is located on a center of inversion and is bound by two terminally bound azido-N9 atoms, two μ_2-azido-N6 atoms where atom N6 bridges

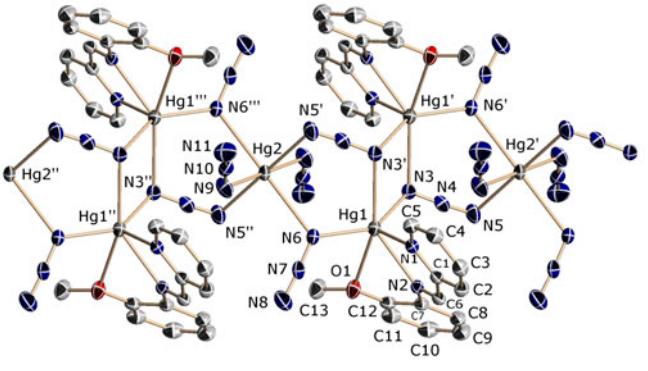

Figure 4. Perspective view of the polymeric chain found in the crystal structure of $\{[HgL^1(N_3)_2]_2{\cdot}Hg(N_3)_2\}_n$ (**2**). Displacement ellipsoids are drawn at the 50% probability level and hydrogen atoms are omitted. Singly, doubly, and triply primed atoms are related by the symmetry operations $1-x$, $-y$, $1-z$, $1+x$, y, z, and $2-x$, $-y$, $1-z$, respectively.

Table 4. Selected bond lengths (Å) and angles (°) for **2**.[a]

Hg(1)–N(1)	2.402(3)	N(1)–Hg(1)–O(1)	120.51(8)
Hg(1)–N(2)	2.453(3)	N(2)–Hg(1)–N(3)	92.00(10)
Hg(1)–N(3)	2.184(3)	N(2)–Hg(1)–N(6)	119.65(11)
Hg(1)–N(6)	2.138(3)	N(2)–Hg(1)–N(3′)	141.38(8)
Hg(1)–N(3′)	2.806(3)	N(2)–Hg(1)–O(1)	58.11(7)
Hg(1)–O(1)	2.926(2)	N(3)–Hg(1)–N(6)	137.83(12)
Hg(2)–N(6)	2.710(3)	N(3)–Hg(1)–N(3′)	77.25(10)
Hg(2)–N(9)	2.069(3)	N(3)–Hg(1)–O(1)	94.72(9)
Hg(2)–N(5′)	2.756(3)	N(6)–Hg(1)–N(3′)	90.67(10)
		N(6)–Hg(1)–O(1)	81.62(10)
N(1)–Hg(1)–N(2)	68.71(9)	N(3′)–Hg(1)–O(1)	158.05(8)
N(1)–Hg(1)–N(3)	112.62(9)	N(6)–Hg(2)–N(9)	94.56(13)
N(1)–Hg(1)–N(6)	105.01(11)	N(6)–Hg(2)–N(5′)	87.87(10)
N(1)–Hg(1)–N(3′)	81.31(9)	N(9)–Hg(2)–N(5′)	90.25(11)

[a]Symmetry operation for primed atoms = $1-x$, $-y$, $1-z$.

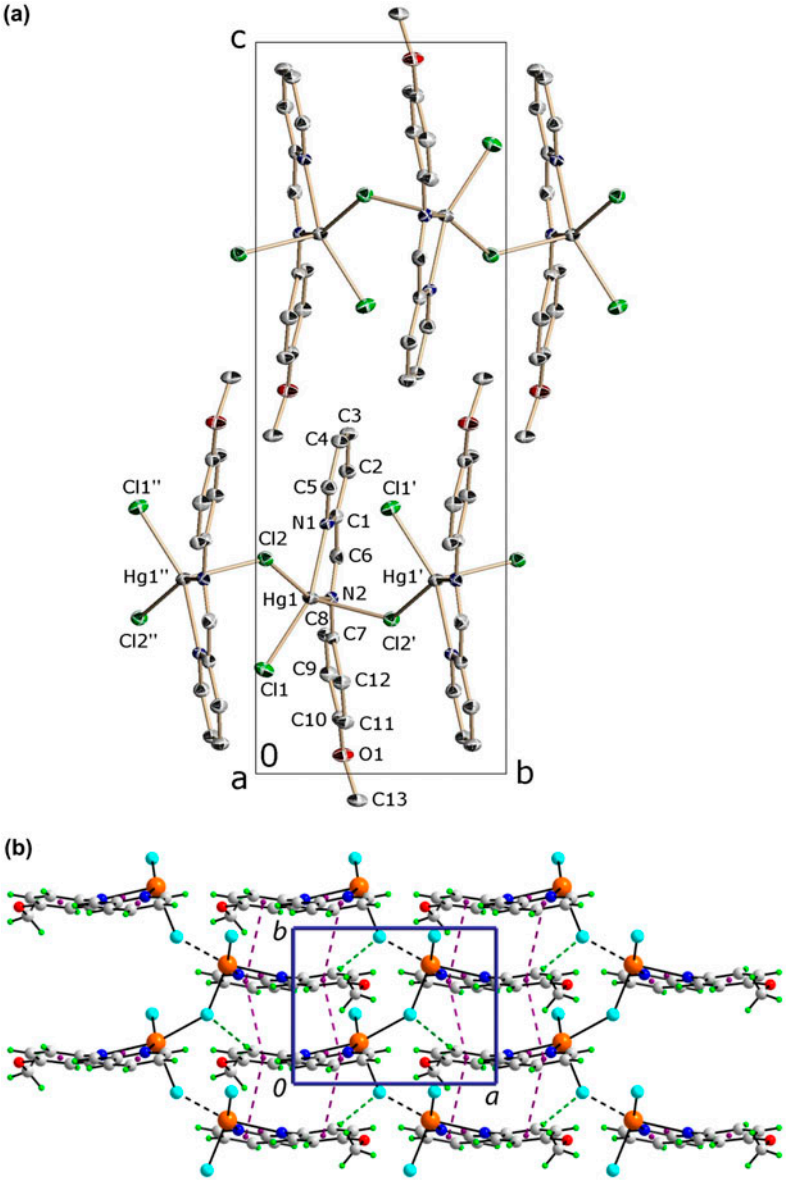

Figure 5. (a) View down the *a*-axis of the unit cell contents of $[HgL^2(Cl)_2]_n$ (**3**) showing the weakly associated extended chain. Displacement ellipsoids are drawn at the 50% probability level and hydrogen atoms are omitted. The primed and doubly primed atoms are related by the symmetry operations $1-x$, $½+y$, $1½-z$, and $1-x$, $-½+y$, $1½-z$, respectively. (b) A view of the supramolecular layer in the *ab*-plane sustained by C–H···Cl hydrogen bonds [C8–H8···Cl2^{i}: H8···Cl2^{i} = 2.73 Å, C8···Cl2^{i} = 3.543(5) Å, angle at H5 = 144° for i: $2-x$, $½+y$, $1½-z$] and π–π interactions [Cg(N1,C1–C5)···Cg(C7–C12)^{ii,iii} = 3.631(3) Å and 3.738(3) Å, angle of inclination = 2.2(2)° in each case, for ii: $2-x$, $-½+y$, $-1½-z$; and iii: $2-x$, $½+y$, $1½-z$] are shown as green and purple dashed lines, respectively (see http://dx.doi.org/10.1080/00958972.2014.901508 for color version).

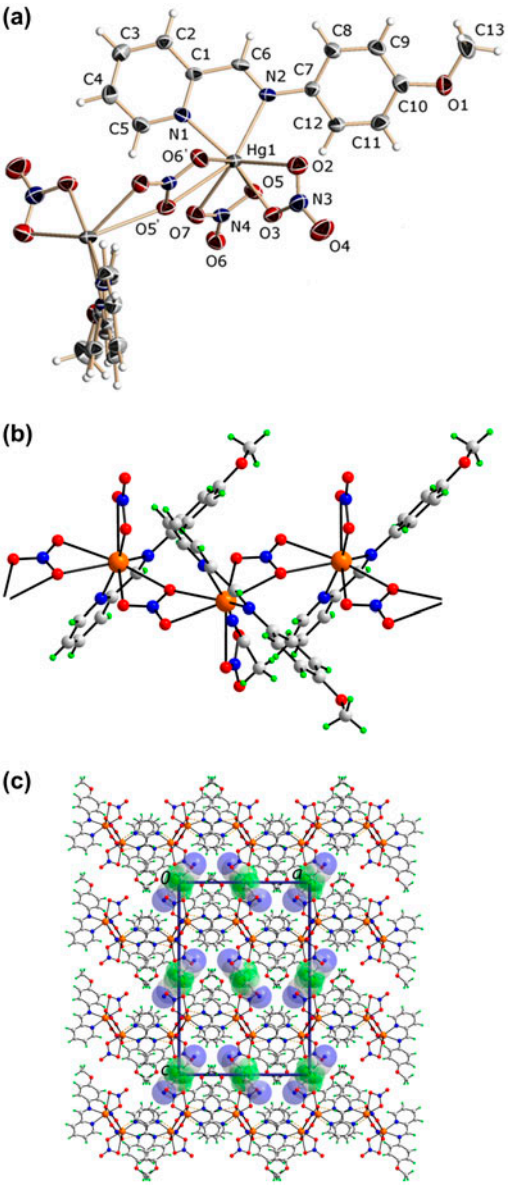

Figure 6. (a) Perspective view of a portion of the polymeric chain illustrated to show the coordination geometry about the mercury(II) atom found in the crystal structure of $[HgL^2(NO_3)_2]_n \cdot nCH_3CN$ (**4**); the acetonitrile molecule is omitted. Displacement ellipsoids are drawn at the 50% probability level and hydrogen atoms are shown as small spheres of arbitrary radii. Primed atoms are related by the symmetry operation $-x, -\frac{1}{2}+y, \frac{1}{2}-z$. (b) The helical coordination polymer mediated by tetradentate nitrate anions. (c) A view in projection down the *b*-axis of the unit cell contents. The supramolecular layers are sustained by C–H···O interactions [C2–H2···O7^{i}: H2···O7^{i} = 2.50 Å, C2···O7^{i} = 3.413(7) Å, angle at H2 = 162°; C6–H6···O6^{i}: H6···O6^{i} = 2.59 Å, C6···O6^{i} = 3.515(6) Å, angle at H6 = 165° for i: $\frac{1}{2}+x, y, \frac{1}{2}-z$] shown as orange dashed lines. The acetonitrile molecules, shown in space-filling mode, are connected to the layers by methyl-C–H···O(nitrate) interactions [C14–H142···O2^{ii}: H142···O2^{ii} = 2.56 Å, C14···O2^{ii} = 3.381(9) Å, angle at H142 = 141° for ii: $\frac{1}{2}+x, \frac{1}{2}-y, -z$] (see http://dx.doi.org/10.1080/00958972.2014.901508 for color version).

across to Hg1, and two azido-N5 atoms where the azido-N3 atom at the other end provides the bridge between Hg1 of the centrosymmetric dimer, hence this ligand is μ_3-bridging. In the dimer, Hg1 and Hg1′ are connected by a pair of end-on bridging azides, via N3 and N3′ (the N5 atoms of these azides form bridges to the Hg2 atoms in the $Hg(N_3)_2$ units), the second azido-N6 is bound end-on and bridges to an adjacent Hg2, and tridentate L^1 coordinates as found in **1**. Hg1 and Hg2 exist in octahedral coordination geometries, at least to a first approximation. For Hg1, two of the bond lengths are considerably longer than the others, e.g. the central core is trapezoidal as the Hg1–N3,N3′ bond lengths differ by about 0.6 Å, and the Hg–O1 distance is also long (table 4). Further distortions arise as a result of the acute chelate angles. While the angles around Hg2 are close to 90° two of the Hg–N9 bond lengths are considerably shorter, by over 0.7 Å, than the remaining four bonds. The result of the azide-mediated bridging is the formation of a coordination polymer aligned along the *a*-axis. Chains stack with no specific intermolecular interactions between them.

The next structure to be described is that of $[HgL^2(Cl)_2]_n$ (**3**), where the methoxy substituent is no longer proximate to the mercury(II) atom so that a Hg–O1 bond is not formed. Instead, the mercury(II) atom increases its coordination number leading to a square pyramidal coordination geometry ($\tau = 0.02$, Cl2 in the axial position) by forming a significant intermolecular Hg1···Cl2 interaction (2.7874(11) Å for symmetry operation $1 - x$, $\frac{1}{2} + y$, $1\frac{1}{2} - z$) resulting in a helical supramolecular chain along the *b*-axis [figure 5(a)]. The chains are connected by C8–H···Cl2 hydrogen bonds as well as π–π interactions between pyridyl and phenyl rings to form a supramolecular array in the *ab*-plane [figure 5(b)]. Layers stack with no specific intermolecular interactions between them.

The mercury(II) atom in polymeric $[HgL^2(NO_3)_2]_n \cdot nCH_3CN$ (**4**) [figure 6(a)] is eight coordinate being chelated by L^2, and coordinated by six nitrate oxygen atoms. The N3-nitrate chelates in an asymmetric mode with the Hg–O3 bond length being 0.6 Å shorter than Hg–O2 (table 5). The N4-nitrate anion bridges two mercury(II) ions, simultaneously chelating both with O5 forming two Hg–O bonds. Reflecting the higher denticity of the

Table 5. Selected bond lengths (Å) and angles (°) for **4** and **5**.[a]

	4	**5**		**4**	**5**
Hg(1)–O(2)	2.757(5)	2.623(3)	O(3)–Hg(1)–O(5)	80.86(14)	74.57(11)
Hg(1)–O(3)	2.157(4)	2.599(3)	O(3)–Hg(1)–O(7)	85.10(15)	119.40(10)
Hg(1)–O(5)	2.731(4)	2.393(3)	O(3)–Hg(1)–N(1)	167.09(17)	138.07(10)
Hg(1)–O(7)	2.587(4)	2.712(3)	O(3)–Hg(1)–N(2)	118.92(17)	95.54(10)
Hg(1)–N(1)	2.200(5)	2.259(3)	O(5)–Hg(1)–O(7)	47.92(12)	49.40(11)
Hg(1)–N(2)	2.398(4)	2.431(3)	O(5)–Hg(1)–N(1)	103.97(15)	102.67(11)
C(1)–C(6)	1.487(8)	1.473(5)	O(5)–Hg(1)–N(2)	90.15(15)	160.11(11)
N(2)–C(6)	1.272(7)	1.277(5)	O(7)–Hg(1)–N(1)	89.37(16)	82.30(11)
N(2)–C(7)	1.416(7)	1.417(4)	O(7)–Hg(1)–N(2)	129.66(14)	144.86(10)
Hg(1)–O(*x*)	2.924(4)	2.229(3)	N(1)–Hg(1)–N(2)	73.41(16)	72.93(10)
Hg(1)–O(6′)	2.725(4)	–	O(2)–Hg(1)–O(*x*)	100.03(12)	129.49(10)
			O(3)–Hg(1)–O(*x*)	84.22(14)	80.66(10)
O(2)–Hg(1)–O(3)	50.81(15)	49.04(9)	O(5)–Hg(1)–O(*x*)	115.21(11)	95.82(11)
O(2)–Hg(1)–O(5)	116.33(13)	77.18(11)	O(7)–Hg(1)–O(*x*)	68.28(12)	83.68(11)
O(2)–Hg(1)–O(7)	135.80(14)	121.49(10)	N(1)–Hg(1)–O(*x*)	82.89(14)	140.24(11)
O(2)–Hg(1)–N(1)	132.82(16)	89.17(10)	N(2)–Hg(1)–O(*x*)	149.00(12)	99.58(10)
O(2)–Hg(1)–N(2)	82.62(15)	83.31(10)	O(2)–Hg(1)–O(6′)	69.77(13)	–
O(3)–Hg(1)–O(6′)	90.24(15)	–	O(5)–Hg(1)–O(6′)	159.46(11)	–
O(7)–Hg(1)–O(6′)	113.22(13)	–	N(1)–Hg(1)–O(6′)	81.22(14)	–
N(2)–Hg(1)–O(6′)	110.32(13)	–	O(x)–Hg(1)–O(6′)	45.00(11)	–

[a] $x = 5'$ for **4** and $x = 8$ for **5**. Symmetry operation for primed atoms = $-x$, $-\frac{1}{2} + y$, $\frac{1}{2} - z$.

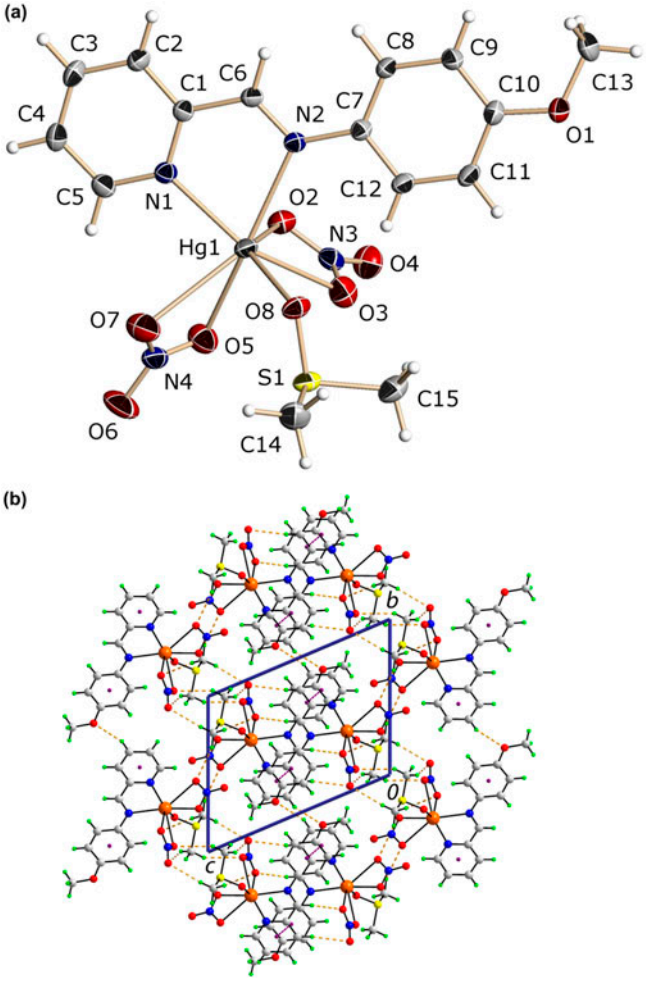

Figure 7. (a) Perspective view of the monomer found in the crystal structure of $[HgL^2(NO_3)_2(DMSO)]$ (**5**). Displacement ellipsoids are drawn at the 50% probability level and hydrogen atoms are shown as small spheres of arbitrary radii. (b) A view in projection down the *a*-axis of the unit cell contents. The π–π interactions [Cg(N1,C1–C5)···Cg(C7–C12)^{i} = 3.763(2) Å, angle of inclination = 2.05(19)° for i: $1-x$, $1-y$, $1-z$] are shown as purple dashed lines. The C–H···O interactions [C3–H3···O1^{ii}: H3···O1^{ii} = 2.60 Å, C3···O1^{ii} = 3.508(5) Å, angle at H3 = 160°; C2–H2···O4^{iii}: H2···O4^{iii} = 2.52 Å, C2···O4^{iii} = 3.463(5) Å, angle at H2 = 173°; C6–H6···O2^{iii}: H6···O2^{iii} = 2.42 Å, C6···O2^{iii} = 3.252(5) Å, angle at H6 = 146°; C14–H142···O4^{iv}: H142···O4^{iv} = 2.51 Å, C14···O4^{iv} = 3.477(6) Å, angle at H142 = 169°; C15–H153···O4^{v}: H153···O4^{v} = 2.50 Å, C15···O4^{v} = 3.400(6) Å, angle at H153 = 152°. Symmetry operations ii: $1+x$, $1+y$, z; iii: $1-x$, $1-y$, $1-z$; iv: $-x$, $-y$, $-z$; v: $-1+x$, y, z] are shown as orange dashed lines (see http://dx.doi.org/10.1080/00958972.2014.901508 for color version).

N4-nitrate anion, the Hg–O bond lengths are long and span 2.587(4)–2.924(4) Å. The disparity in the bond lengths about the mercury(II) atom, along with the acute chelate angles, leads to a highly distorted coordination geometry. One description is based on a square anti-prism with one face (distinctly rectangular, defined by the O2, O3, O5′, and O6 atoms) being twisted about 7° with respect to the other (distinctly trapezoidal, defined by O5, O7, N1, and N2). The result of the tetradentate and bridging N4-nitrate ligand is the

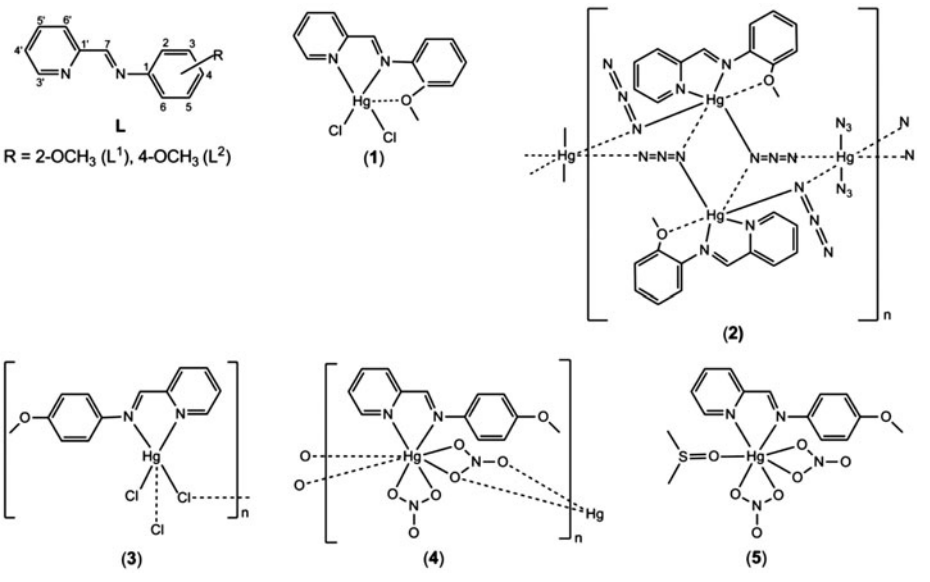

Scheme 1. The ligands L^1–L^2 and the investigated compounds **1**–**5**.

formation of a helical coordination polymer along the *b*-axis as illustrated in figure 6(b). When viewed down the direction of the polymer, the global crystal packing can be described as undulating layers of polymers stacked along the *c*-axis [figure 6(c)] and acetonitrile solvent molecules lie in the interlayer region. Connections within layers are of the type methyl-C–H···O(nitrate), as are those between the solvent and layer.

Recrystallization of **4** from DMSO yielded **5**, formulated as $[HgL^2(NO_3)_2(DMSO)]$, which is monomeric and features O-bound DMSO [figure 7(a)]. Both nitrates are chelating with Hg–O bond lengths ranging from 2.393(3) to 2.712(3) Å, i.e. within the range of comparable bonds in **4** (table 5). The L^2 ligand is also chelating and the Hg–N1, N2 bond lengths are longer than those in **4**, reflecting more tightly bound nitrates and also the strong Hg–O8 bond of 2.229(3) Å involving the DMSO oxygen atom. With three acute angles provided by the chelating ligands, not surprisingly the coordination polyhedron is highly distorted. One description is based on a capped octahedron. The axial angle of 160.11(11) is subtended by atoms O5 and N2 atom, the approximate basal plane is defined by atoms O2, O3, O8, and N1, leaving O7 to occupy the triangular face defined by atoms O5, O8, and N1. In the crystal packing, a pair of π–π interactions occurring between the pyridyl and phenyl rings of centrosymmetrically related molecules leads to the formation of loosely associated dimeric units. The dimeric aggregates stack in columns along the *a*-axis and are connected into a 3-D architecture by C–H···O interactions [figure 7(b)] involving nitrate-O as acceptors, as for **4**, the methoxy-O as an acceptor, and L^2- and DMSO-methyl-H as donors.

4. Conclusion

Five neutral $[HgL^1(Cl)_2]$ (**1**), $\{[HgL^1(N_3)_2]_2{\cdot}Hg(N_3)_2\}_n$ (**2**), $[HgL^2(Cl)_2]_n$ (**3**), $[HgL^2(NO_3)_2]_n{\cdot}nCH_3CN$ (**4**), and $[HgL^2(NO_3)_2(DMSO)]$ (**5**) compounds of bidentate NN and tridentate NNO donor Schiff-base ligands have been synthesized. The compounds were

characterized by spectroscopic and single crystal X-ray crystallographic techniques. The crystal structures revealed the presence of monomeric (**1**, **3**, and **5**) and polymeric (**2** and **4**) species in the solid state. The appearance of monomeric **1** and **5** is correlated with the additional coordination, intra- and intermolecularly, by oxygen which reduces the Lewis acidity of the mercury(II) centre. In the absence of additional Hg–O bonds, polymeric structures arise via bridging azide, chloride, and nitrate in **2**, **3**, and **4**, respectively.

Supplementary material

CCDC 970664–970668 contains the supplementary crystallographic data for **1–5**. These data can be obtained free of charge via http://www.ccdc.cam.ac.uk/conts/retrieving.html or from the Cambridge Crystallographic Data Centre, 12 Union Road, Cambridge CB2 1EZ, UK; Fax: +44 1223 336 033; or E-mail: deposit@ccdc.cam.ac.uk.

Acknowledgements

The financial support of the University Grants Commission, New Delhi, India (F. No. 42-396/2013 (SR) TSBB) and the Indo-Swiss Joint Research Programme, Joint Utilisation of Advanced Facilities [grant number JUAF 11, TSBB, AL] are gratefully acknowledged. Support from the Ministry of Higher Education, Malaysia, and the University of Malaya, for High Impact Research grant [UM.C/HIR-MOHE/SC/03] is also gratefully acknowledged. The authors gratefully acknowledge access to the X-ray facilities in the Chemical Research Center at the Autonomous State University of Morelos (CIQ-UAEM).

References

[1] E.F. DiMauro, M.C. Kozlowski. *Org. Lett.*, **3**, 1641 (2001).
[2] R. Clérac, H. Miyasaka, M. Yamashita, C. Coulon. *J. Am. Chem. Soc.*, **124**, 12837 (2002).
[3] M.R. Maurya, A. Kumar, A.R. Bhat, A. Azam, C. Bader, D. Rehder. *Inorg. Chem.*, **45**, 1260 (2006).
[4] T. Glaser, I. Liratzis, O. Kataeva, R. Fröhlich, M. Píacenza, S. Grimme. *Chem. Commun.*, 1024 (2006).
[5] A.R. Stefankiewicz, M. Wałęsa-Chorab, H.B. Szcześniak, V. Patroniak, M. Kubicki, Z. Hnatejko, J. Harrowfield. *Polyhedron*, **29**, 178 (2010).
[6] T. Katsuki. *Coord. Chem. Rev.*, **140**, 189 (1995).
[7] P.J. Pospisil, D.H. Carsten, E.N. Jacobsen. *Chem. Eur. J.*, **2**, 974 (1996).
[8] T. Thanyasiri, E. Sinn. *J. Chem. Soc., Dalton Trans.*, 1187 (1989).
[9] L. Canali, D.C. Sherrington. *Chem. Soc. Rev.*, **28**, 85 (1999).
[10] T.S. Basu Baul, S. Kundu, S. Mitra, H. Höpfl, E.R.T. Tiekink, A. Linden. *Dalton Trans.*, 1905 (2013).
[11] T.S. Basu Baul, S. Kundu, H. Höpfl, E.R.T. Tiekink, A. Linden. *Polyhedron*, **55**, 270 (2013).
[12] A.J. Bloodworth. *J. Organomet. Chem.*, **23**, 27 (1970).
[13] Agilent Technologies. *CrysAlisPro (Version 1.171.33.55)*, Yarnton, Oxfordshire (2010).
[14] R. Hooft. *KappaCCD Collect Software*, Nonius BV, Delft (1999).
[15] Bruker Analytical X-ray Systems. *SAINT-NT (Version 6.04)*, Madison, Wisconsin, USA (2001).
[16] Z. Otwinowski, W. Minor. *Methods in Enzymology*. In *Macromolecular Crystallography, Part A*. C.W. Carter Jr and R.M. Sweet (Eds), Vol. 276, pp. 307–326, Academic Press, New York (1997).
[17] R.H. Blessing. *Acta Crystallogr., Sect A*, **51**, 33 (1995).
[18] R.C. Clark, J.S. Reid. *Acta Crystallogr., Sect A*, **51**, 887 (1995).
[19] P.T. Beurskens, G. Admiraal, G. Beurskens, W.P. Bosman, S. Garcia-Granda, R.O. Gould, J.M.M. Smits, C. Smykalla. *PATTY: The DIRDIF Program System, Technical Report of the Crystallography Laboratory*, University of Nijmegen, Nijmegen (1992).
[20] Bruker Analytical X-ray Systems. *SHELXTL-NT (Version 6.10)*, Madison, Wisconsin, USA (2000).
[21] G.M. Sheldrick. *Acta Crystallogr., Sect. A*, **64**, 112 (2008).
[22] S.S. Tandon, S. Chander, L.K. Thompson. *Inorg. Chim. Acta*, **300–302**, 683 (2000).

[23] K. Nakamoto. *Infrared and Raman Spectra of Inorganic and Coordination Compounds*, Wiley, New York (1986).
[24] G. Mahmoudi, A. Morsali. *Polyhedron*, **27**, 1070 (2008).
[25] J. Ribas, A. Escuer, M. Monfort, R. Vicente, R. Cortés, L. Lezama, T. Rojo. *Coord. Chem. Rev.*, **193–195**, 1027 (1999).
[26] U.S. Ray, B.G. Chand, G. Mostafa, J. Cheng, T.-H. Lu, C. Sinha. *Polyhedron*, **22**, 2587 (2003).
[27] G.J. Kleywegt, W.G.R. Wiesmeijer, G.J. Van Driel, W.L. Driessen, J. Reedijk, J.H. Noordik. *J. Chem. Soc., Dalton Trans.*, 2177 (1985).
[28] A.K. Boudalis, V. Nastopoulos, S.P. Perlepes. *Transition Met. Chem.*, **26**, 276 (2001).
[29] P. Biscarini, L. Fusina, G.D. Nivellini. *J. Chem. Soc., Dalton Trans.*, 1003 (1972).
[30] K. Nakamoto. *Infrared and Raman Spectra of Inorganic and Coordination Compounds*, 6th edn, Part B, Wiley, Hoboken, NJ (2009).
[31] T.K. Chattopadhyay, A.K. Kumar, A. Roy, A.S. Batsanov, E.B. Shamuratov, Yu.T. Struchkov. *J. Organomet. Chem.*, **419**, 277 (1991).
[32] S. Basu Baul, T.S. Basu Baul, E. Rivarola, D. Dakternieks, E.R.T. Tiekink, A. Chatterjee, C. Sing-ai. *Appl. Organomet. Chem.*, **12**, 503 (1998).
[33] C. Seward, J. Chan, D. Song, S.-N. Wang. *Inorg. Chem.*, **42**, 1112 (2003).
[34] (a) R.S. Drago. *Physical Methods in Chemistry*, Chap. 5, Saunders, Philadelphia, PA (1977); (b) F. Masetti, U. Mazzucato, G. Galiazzo. *J. Lumin.*, **4**, 8 (1971); (c) T.C. Warner, W. Hawkins, J. Facci, R. Torrisi, T. Trembath. *J. Phys. Chem.*, **82**, 298 (1978); (d) M.C. Aragoni, M. Arca, F. Demartin, F.A. Devillanova, F. Isaia, A. Garau, V. Lippolis, F. Jalali, U. Papke, M. Shamsipur, L. Tei, A. Yari, G. Verani. *Inorg. Chem.*, **41**, 6623 (2002).
[35] A.W. Addison, T.N. Rao, J. Reedijk, J. van Rijn, G.C. Verschoor. *J. Chem. Soc., Dalton Trans.*, 1349 (1984).
[36] J. Gans, D. Shalloway. *J. Mol. Graphics Modell.*, **19**, 557 (2001).
[37] K. Brandenburg. *DIAMOND*, Crystal Impact GbR, Bonn (2006).
[38] Z.D. Tomić, D.N. Sredojević, S.D. Zarić. *Cryst. Growth Des.*, **6**, 29 (2006).
[39] D.N. Sredojević, Z.D. Tomić, S.D. Zarić. *Cryst. Growth Des.*, **10**, 3901 (2010).
[40] E.R.T. Tiekink. In *Crystal Engineering. Supramolecular Chemistry: From Molecules to Nanomaterials*, J.W. Steed, P.A. Gale (Eds), John Wiley, Chichester (2012), p. 2791.